Isotope shifts and hyperfine-structure-splitting constants of the 4*d*-5*p* transition of Kr II at $\lambda = 729$ nm

H. A. Schuessler
Department of Physics, Texas A&M University, College Station, Texas 77843

A. Alousi
Foster Radiation Laboratory, McGill University, Montreal, Canada H3A 2B2

M. Idrees
Department of Physics and Chemistry, Southeastern Louisiana University, Hammond, Louisiana 70402

Y. F. Li
Department of Physics, Texas A&M University, College Station, Texas 77843

F. Buchinger
Foster Radiation Laboratory, McGill University, Montreal, Canada H3A 2B2

R. M. Evans
Department of Physics, Texas A&M University, College Station, Texas 77843

C. F. Fischer
Department of Computer Science, Vanderbilt University, Nashville, Tennessee 37235
(Received 5 December 1991)

Collinear fast-beam laser spectroscopy has been used to measure the hyperfine splittings and the isotope shifts in the $4p^4 4d\ ^4D_{7/2}-4p^4 5p\ ^4P^\circ_{5/2}$ ($\lambda = 729$ nm) transition of singly ionized Kr. The measured isotope shifts are very large due to a large specific-mass effect that is caused by the strong momentum correlations of the 4*d* electron with the core electrons. Hartree-Fock and multiconfiguration Hartree-Fock (MCHF) calculations of the specific-mass shift were carried out and are compared to the measurements. The MCHF calculation yields excellent agreement with the experimental results.

PACS number(s): 35.10.Fk, 32.30.Jc, 31.50.+w

I. INTRODUCTION

Renewed interest in optical spectroscopy of stable krypton isotopes has centered on high-resolution measurement of hyperfine-splitting (HFS) parameters and isotope shifts (IS) [1–4]. On one hand, some of these studies were motivated by the search for ultrasensitive detection schemes capable of counting a few krypton atoms or of detecting trace quantities of a specific krypton isotope (e.g., the long-lived isotopes ^{81}Kr and ^{85}Kr) in samples containing much larger amounts of the stable isotopes. These detection schemes are of interest in many applications, including dating, environmental monitoring, solar neutrino flux measurements, double β-decay studies, and low-level neutron dosimetry [1,5–18]. On the other hand, other spectroscopic measurements [1–4] concentrated on improving the understanding of the atomic structure of krypton in general. They provide the data necessary for performing parametric analyses and for checking and refining *ab initio* atomic-structure calculations, such as Hartree-Fock (HF), multiconfiguration Hartree-Fock (MCHF), and many-body perturbation theory (MBPT). In all cases, a detailed knowledge of the atomic spectrum of Kr is essential.

Up to now most of the spectroscopic data available have been obtained in neutral Kr (Kr I) [1,3,4]. For singly ionized krypton (Kr II), only HFS results from a study of the $4d\ ^4D_{7/2}-5p\ ^4D^\circ_{7/2}$ ($\lambda = 642$ nm) transition had been reported [2], thus offering a very limited database for theoretical investigations. In this paper we extend the spectroscopic information on Kr II by reporting on measurements of the HFS and IS in the Kr II $4d\ ^4D_{7/2}-5p\ ^4P^\circ_{5/2}$ ($\lambda = 729$ nm) transition using the fast-beam collinear laser spectroscopy method. The results described in the present work include a first measurement of an isotope shift in the Kr II spectrum. A preliminary account of this work has already appeared [19] elsewhere.

Analogous *d*-*p* transitions in the ionic spectra of other noble gases were investigated in Ar [20] and Xe [21,22]. The data reveal a large specific-mass shift (SMS), several times the size of the normal-mass shift (NMS). Hence, transitions of this type are particularly suitable for testing the reliability of *ab initio* calculations of the SMS.

The uncertainty involved in estimating the size of the SMS contribution to the IS is often the factor limiting the accuracy with which changes in nuclear mean-square charge radii can be extracted from optical IS measurements [23]. This is especially true for light and medium

 ©1992 The American Physical Society

heavy elements. Therefore, the availability of a reliable method for calculating the SMS can be of crucial importance in such studies. We have carried out HF and MCHF calculations of the SMS for the transition investigated. These calculations are presented in Sec. III. A description of the apparatus and the experimental results are presented in Sec. II.

II. EXPERIMENTAL PROCEDURE AND RESULTS

The collinear fast-beam laser spectroscopy method [24] was used to measure isotope shifts and hyperfine structures in the Kr II $4d\,^4D_{7/2}-5p\,^4P^{\circ}_{5/2}$ ($\lambda=729$ nm) transition. The apparatus is a slightly modified version of the one described briefly in a report on a recent on-line experiment [25] on the short-lived neutron-rich isotopes ^{88}Kr and ^{90}Kr. A schematic view of the apparatus is shown in Fig. 1.

The ion source used to produce Kr ions is a Colutron-type plasma ion source [26]. High-purity Kr gas, containing all the stable isotopes in their natural abundances (^{86}Kr, 17.3%; ^{84}Kr, 57%; ^{83}Kr, 11.5%; ^{82}Kr, 11.6%; ^{80}Kr, 2.25%; ^{78}Kr, 0.35%), is introduced into the source. The plasma is created by an arc discharge inside the source. Metastable states in the Kr ion are excited by electron impact in the plasma. The fraction of ions leaving the source in a metastable state is dependent on the ion-source operating parameters [27]. In our experiment the ion-source discharge voltage and current were set to match the conditions for optimum metastable state population [27]. Under these conditions, the fraction of ions exiting the source in one of the metastable states of Kr II, including the $4d\,^4D_{7/2}$ state, is about 1% [27]. The singly ionized, unseparated beam is extracted from the source and accelerated to energies between 4 and 5 keV. The ion beam is then merged collinearly with the laser beam by deflecting it through an angle of about 3° using a set of bending capacitors. A quadrupole triplet lens and two sets of horizontal and vertical deflection plates allow the optimization of both the ion-beam transmission through the apparatus and its overlap with the laser in the observation region. The ion beam is counterpropagating with a cw laser beam. Light of wavelength $\lambda=729$ nm is obtained from a frequency-stabilized single-mode ring dye laser (Spectra Physics Model No. 380D) operating on Pyridine 1 or Styryl 8 dye. Typical laser powers used during the experiment were 2 to 3 mW.

Excitation in the $\lambda=729$-nm transition is achieved by Doppler tuning the ions through resonance at a fixed laser frequency. For this purpose a variable voltage is applied to a Faraday cage located at the center of the light collection system. A slot is machined in each side of the Faraday cage allowing the imaging system to view an observation region about 3 cm long, along the ion beam. The transition from the metastable initial $4d\,^4D_{7/2}$ state to the $5p\,^4P^{\circ}_{5/2}$ excited state at $\lambda=729$ nm is observed by detecting the fluorescence photons from the $\lambda=474$-nm and $\lambda=531$-nm lines to the $5s\,^4P_{3/2,5/2}$ states (see Fig. 2). The light collection system consists of a spherical concave mirror and a pair of Fresnel lenses which focus the light onto the photocathode of a cooled photomultiplier tube (RCA Model No. 31034-2). A dichroic filter (OCLI Stock Blue Filter) with a cutoff near $\lambda=500$ nm reduces the background from laser stray light and collisional excitation of the rest gas in the observation region. The solid angle of acceptance of the light collection system is 3% of 4π.

The experiment is controlled by an IBM personal computer interfaced via a CAMAC system. A scan voltage is supplied by a digital-to-analog converter (DAC) [Kinetic Systems Model No. 3112, 12-bit D/A (digital-analog) converter; output, -2.5 to $+2.5$ V] to the input of an operational power supply (Kepco Model No. BOP 1000 M) which amplifies the DAC output by a factor of 100. This variable voltage (i.e., the output of the operational power supply) is then superimposed on an adjustable dc voltage and the sum is applied to the Faraday cage con-

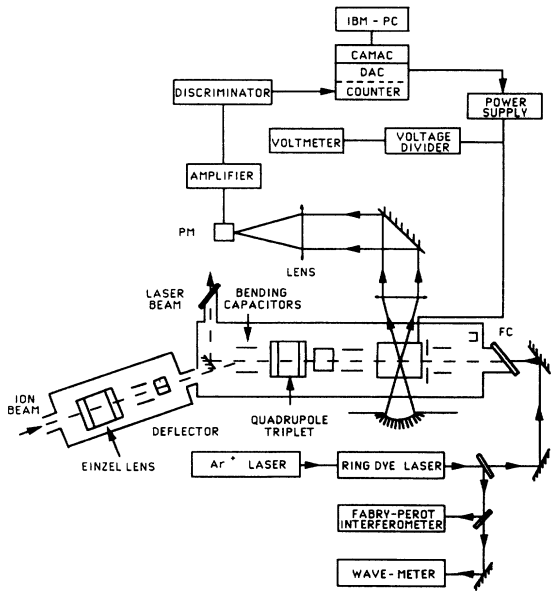

FIG. 1. Schematic view of the collinear fast-beam laser spectroscopy setup used in the experiment.

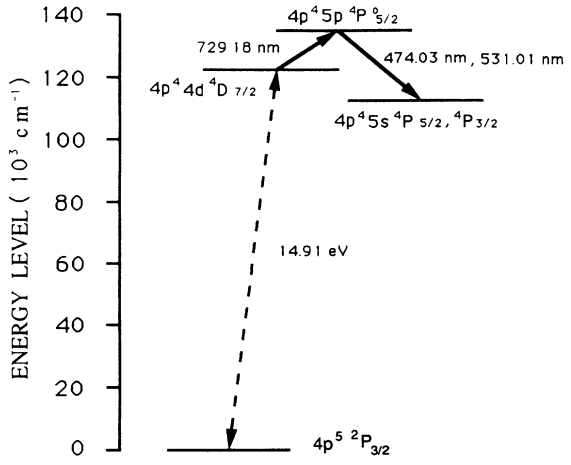

FIG. 2. The excitation-observation scheme used for spectroscopy in the $\lambda=729$-nm line.

taining the observation region. The sum voltage is measured using a $10k$:1 voltage divider (Julie Research Laboratories Model No. KV10R) and a microvolt digital multimeter (Keithley Model No. 197). Start and stop voltages at either end of the scan are recorded before and after each measuring cycle which typically includes ten scans. The uncertainty in this voltage measurement is estimated to be 0.1 to 0.2 V. Similarly, the acceleration voltage applied to the ion source is measured using a $1k$:1 voltage divider (Julie Research Laboratories Model No. KV-VB-10) and a digital multimeter (PREMA Model No. 6040S). The accuracy with which this high voltage is measured is about 1 V. Pulses from the photomultiplier tube are amplified and then counted in a 100-MHz counter (Kinetic Systems Model No. 3615). The output of this counter is read by the personal computer through the CAMAC interface (Transiac Model No. 6002).

Several runs were carried out for the measurement of the hyperfine structure and isotope shifts in the Kr II line. Intensities of the ion beams used were of the order of 100 nA. The ion beam was not mass separated (i.e., contained all stable Kr isotopes) and consisted of ions in the ground and metastable states. A typical spectrum, showing the laser-induced fluorescence signals from all stable Kr isotopes, is shown in Fig. 3. The even isotopes exhibit single lines. The odd isotope ^{83}Kr displays HFS splittings. All of the 18 hyperfine-structure components in the spectrum of ^{83}Kr ($I=\frac{9}{2}$) were observed and identified. Most of the components are well resolved in the spectrum shown. Components obscured in this spectrum under the large signals from the even isotopes could be observed in runs where different voltages were applied to the ion source. The linewidth was measured to be 45 MHz full width at half maximum (FWHM). It is due to contributions from the residual Doppler width and a natural linewidth of $\delta\nu_n=20$ MHz [28]. The residual Doppler width yields an upper limit for the energy spread of the ions leaving the source of $\delta E\approx 2.8$ eV. The background is due mostly to collisional excitation of the rest gas in the observation region.

The difference between the resonant frequencies of two peaks in the spectrum is given by

$$\delta\nu^{A'A}=\nu^{A}-\nu^{A'}=\nu_L\left[\left[\frac{1+\beta^{A}}{1-\beta^{A}}\right]^{1/2}-\left[\frac{1+\beta^{A'}}{1-\beta^{A'}}\right]^{1/2}\right], \tag{1}$$

where $\beta=v/c$ and ν_L is the laser excitation frequency. A and A' are the mass numbers of the isotopes to which the peaks belong. Using this relation, the evaluation of the isotope shifts for the even isotopes from the spectra is straightforward. For the odd isotope ^{83}Kr, the assignment of the different hyperfine components was done relying on the expected intensity ratios [29] and the known hyperfine splitting [2] of the $4d\,^4D_{7/2}$ initial state. The frequencies of the different hyperfine-structure components of ^{83}Kr, relative to ^{84}Kr, were determined using Eq. (1). From this, the various hyperfine splittings in both the $4d\,^4D_{7/2}$ and the $5p\,^4P^{\circ}_{5/2}$ states can be extracted.

The energies W_F of the hyperfine levels are given by

$$W_F=W_J+\tfrac{1}{2}AC+B\frac{\frac{3}{4}C(C+1)-I(I+1)J(J+1)}{2I(2I-1)J(2J-1)} \tag{2}$$

where W_J is the energy of the unperturbed fine-structure level, A and B are the hyperfine-structure constants, I, is the nuclear spin, J is the angular momentum of the atom-

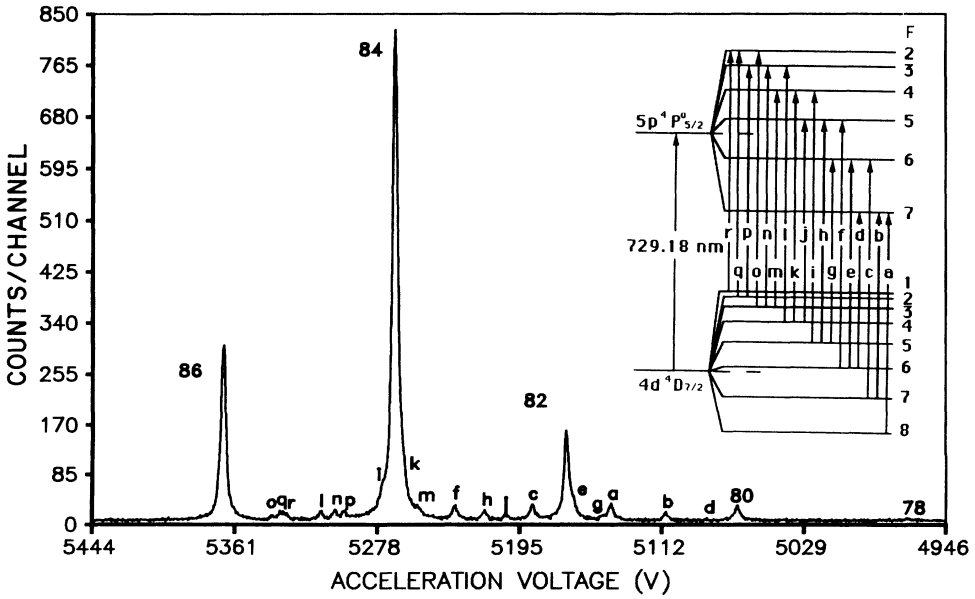

FIG. 3. Spectrum recorded in the $\lambda=729$-nm line. The even isotopes are labeled by their mass number. The HFS components of ^{83}Kr are labeled "a" through "r." The assignments correspond to the HFS transitions sketched in the inset.

ic level, F is the hyperfine quantum number, and

$$C=F(F+1)-I(I+1)-J(J+1)\ .$$

From the measured hyperfine intervals one can solve for A and B. If more than two independent hyperfine splittings are measured in either state, as was the case in the present work, the system is overdetermined and can be solved graphically [3,30]. Once the A and the B values are found for both states, the position of the hyperfine components relative to ^{84}Kr are used to calculate the isotope shift.

The results for the A and B factors of the $5p\ ^4P^\circ_{5/2}$ and $4d\ ^4D_{7/2}$ excited states of ^{83}Kr and the isotope shifts for the stable isotopes between $A=78$ and 86 are compiled in Table I. The uncertainties indicated include statistical and systematic errors. They reflect mainly the accuracy in the determination of the peak positions and in the measurements of the voltages.

In order to estimate the contribution of the mass shift to the observed isotope shift $\delta\nu_{729}$ in the $\lambda=729$-nm line, we use a King-plot procedure [31]. In Fig. 4 the modified isotope shift

$$\delta\nu'_{729}=\delta\nu_{729}[AA'/(A'-A)]$$

is plotted against the corresponding one in the $5s[\frac{3}{2}]^\circ_2-5p[\frac{3}{2}]_2$ ($\lambda=760$ nm) transition [25] in neutral Kr. The slope of the straight line through the data points is given by the ratio [23] of the constants F_{729} and F_{760}, where F is defined by $\delta\nu_{\rm FS}^{AA'}=F\delta\langle r^2\rangle^{AA'}$. $\delta\nu_{\rm FS}$ is the field shift (FS) and $\delta\langle r^2\rangle^{AA'}$ is the change in nuclear mean-square charge radius between the two isotopes with mass numbers A and A'. Therefore, the slope of the line is also proportional to the ratio of the FS in the two lines.

For the series of stable isotopes, the contribution from the FS in the Kr I ($\lambda=760$ nm) line was found to be about 10 MHz for a change of two mass numbers [25]. The slope found in the King plot is $m=-0.5(5)$. This yields an average contribution from the FS of 5(5) MHz per two neutrons to the total isotope shift in the $\lambda=729$-nm line. Comparing this value with the observed total shifts (Table I), we find that the contribution from the FS to the total isotope shift is small and within the experimental error in the IS measurement. Therefore, the FS will be neglected in the discussion below, which concentrates on the specific-mass shift.

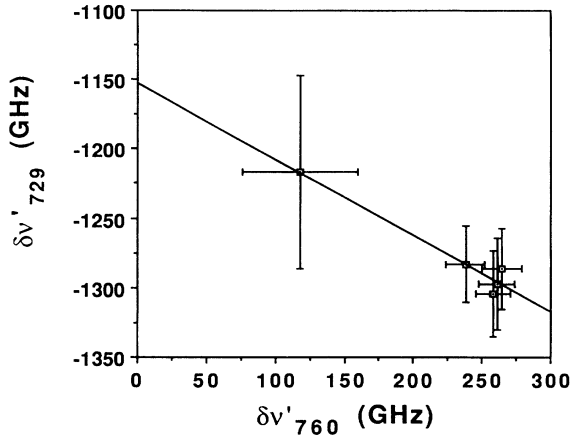

FIG. 4. King plot of the modified isotope shifts $\delta\nu'=\mathrm{IS}(AA')/(A-A')$ in the $\lambda=729$-nm line in ionic Kr vs those in the $5s$-$5p$ ($\lambda=760$ nm) transition in neutral Kr.

Under the above assumption, namely, that the observed IS is totally due to the mass shift, the SMS can be obtained by subtracting the contribution of the normal-mass shift [23] which is calculated according to $\delta\nu_{\rm NMS}^{AA'}=(\nu/1{,}836.15)\ (A'-A)/A'A$, with ν being the atomic transition frequency. The NMS accounts for roughly 65 MHz per two neutrons. The values for the NMS and the SMS are given in the first and the last columns of Table V, respectively. It can be seen that the contribution of the SMS to the total mass shift amounts to roughly seven times the normal-mass contribution. This feature, namely, the predominance of the SMS contribution to the total IS in a p-d transition in Kr II, has also been observed in the ionic spectra of two other noble gases, Ar [20] and Xe [21].

III. CALCULATION OF THE SPECIFIC-MASS SHIFT

The effect of the nuclear motion can be expressed by the additional perturbation H' to the Hamiltonian H_0, with H_0 being the energy operator for an atom with fixed nucleus [32]. This perturbation H' can be split further into two parts, the normal-mass term and the specific-mass term. It is the latter term which gives rise to the

TABLE I. Isotope shifts and HFS parameters obtained in the Kr II $\lambda=729$-nm transition. The A and B factors for the $4p^45p\ ^4P^\circ_{5/2}$ state were evaluated using the HFS parameters for the $4p^45d\ ^4D_{7/2}$ state from Ref. [2]. In addition, the A and B factors for the $^4D_{7/2}$ state were independently determined solely from our measurements.

Isotope shift (MHz)		^{83}Kr hyperfine-structure constants (MHz)	
ν^{86}-ν^{84}	−356.2(8.0)[a]	$A(^4D_{7/2})$	−44(2)[a]
ν^{84}-ν^{83}	−175.0(10.0)[a]		−43.5132(3)[b]
		$B(^4D_{7/2})$	−297(17)[a]
ν^{84}-ν^{82}	−372.6(8.0)[a]		−294.921(5)[b]
ν^{82}-ν^{80}	−395.4(10.0)[a]	$A(^4P^\circ_{5/2})$	−167.2(1.5)[a]
ν^{80}-ν^{78}	−417.7(10.0)[a]	$B(^4P^\circ_{5/2})$	+91(15)[a]

[a]Present work.
[b]Reference [2].

SMS and which must be evaluated for each level separately by the use of the proper atomic wave functions.

The SMS for an atomic state can be expressed as the expectation value of the shift operator [32]:

$$\hat{O}=\frac{-2mR_M}{M}\sum_{\substack{i,j\\ i<j}}(\nabla_i\cdot\nabla_j)\ . \tag{3}$$

The change in the transition energy of a spectral line due to the specific-mass effect, or the observed SMS, is the difference of two such shifts, namely, the shift for the lower state minus that for the upper state. In Eq. (3), m and M denote the mass of an electron and the nucleus, respectively; $R_M=R_\infty/(1+m/M)$ is the Rydberg constant appropriate for the atomic mass M in question; and $\mathbf{p}_i=-i\hbar\nabla_i$ is the momentum of the ith electron. The SMS calculation involves a correlation between two electronic momenta. The problem is compounded further because electron-electron Coulomb effects are important in the precise calculation of the SMS, and these effects are difficult to describe by simple means.

As a first approach to obtaining the SMS in the $4p^4 4d\ ^4D-4p^4 5p\ ^4P$ transition in Kr II, a standard HF calculation was performed. The SMS was obtained by taking the expectation value of the operator in Eq. (3). In this procedure the expectation value can be described in terms of the Vinti integrals [33]

$$\delta\nu_{\rm SMS}=2m\left[\frac{R_M}{M}-\frac{R_{M'}}{M'}\right][J^2(nl,n'l-1)-J'^2(nl,n'l-1)]\ . \tag{4}$$

Hereby the Vinti integrals of the upper state are primed. These integrals were evaluated by making use of the Hartree-Fock spin orbitals. The radial form of the Vinti integral is given by

$$J(nl,n'l-1)=\int_0^\infty R_{n,l}(r)\left[\frac{d}{dr}-\frac{(l-1)}{r}\right]R_{(n',l-1)}(r)r^2dr\ . \tag{5}$$

The results for the Kr II transition investigated are reported in Table II, where the radial Vinti integrals (multiplied by the appropriate angular factors) are listed. The values were compiled to show where the dominant contributions to the SMS arise. It can be seen that the contributions from the core electrons to the SMS do not cancel exactly, but that the dominant corrections come from the outer electrons of the open shells of the lower and upper states.

A much better way to determine the SMS is to use a variational MCHF method [34]. This technique was, therefore, subsequently applied to evaluate the SMS in the Kr II transition of interest. The MCHF method has been known to be successful in predicting many of the properties of ions and neutral atoms [35–37]. In an earlier work, a MCHF evaluation of the SMS was carried out [38] for the ground states of He, Li^+, Be^{2+}, and Ne^{8+}, investigating the accuracy of using different, but equivalent, operator forms of the SMS. It was found that two expressions, namely, the gradient form and the Slater

TABLE II. Contributions from the Vinti integrals for the $4p^4 4d\ ^4D\rightarrow 4p^4 5p\ ^4P$ transition in Kr^+ (in a.u. units).

	Vinti integrals	Contribution
Core contributions		
	$J^2(2p,1s)-J'^2(2p,1s)$	−0.003 917
	$J^2(2p,2s)-J'^2(2p,2s)$	−0.000 055
	$J^2(2p,3s)-J'^2(2p,3s)$	0.001 773
	$J^2(2p,4s)-J'^2(2p,4s)$	0.012 577
	$J^2(3p,1s)-J'^2(3p,1s)$	0.006 518
	$J^2(3p,2s)-J'^2(3p,2s)$	0.005 789
	$J^2(3p,3s)-J'^2(3p,3s)$	0.000 139
	$J^2(3p,4s)-J'^2(3p,4s)$	0.033 839
	$J^2(3d,2p)-J'^2(3d,2p)$	−0.051 817
	$J^2(3d,3p)-J'^2(3d,3p)$	0.006 478
Core-outer contributions		
	$J^2(4p,1s)-J'^2(4p,1s)$	0.156 126
	$J^2(4p,2s)-J'^2(4p,2s)$	0.091 886
	$J^2(4p,3s)-J'^2(4p,3s)$	0.039 649
	$J^2(4p,4s)-J'^2(4p,4s)$	0.007 971
	$J^2(3d,4p)-J'^2(3d,4p)$	0.044 914
	$-J'^2(5p,1s)$	0.083 029
	$-J'^2(5p,2s)$	0.048 944
	$-J'^2(5p,3s)$	0.022 371
	$-J'^2(5p,4s)$	0.001 863
	$-J'^2(3d,5p)$	0.023 910
	$J^2(4d,2p)$	−0.454 819
	$J^2(4d,3p)$	−0.037 987
	$J^2(4d,4p)$	−0.525 193

integral form, agreed very well when the total wave function was nearly exact. However, such accuracy cannot be achieved when more complex atomic systems are considered. Initially, in Ref. [38], the Slater-integral form appeared to yield more accurate results, but subsequent studies, using wave functions of increasing accuracy [39] reported for Li ^2S, have shown the gradient form to be better. Similarly, in a study of core-valence correlation in Ca^+, it was found that results using the gradient form agreed very well with the MBPT calculation [40] whereas the Slater-integral form deviated substantially [41]. For this reason the present calculations are based entirely on the gradient form the SMS operator.

The MCHF method allows the determination of radial functions that define the orbitals of configuration states in the expansion of the nonrelativistic wave function of a many-electron system. In the MCHF approximation, an atomic state describing a many-electron system with total angular and spin momenta LS can be written as

$$\psi = \sum_{i=1}^{m} c_i \Phi(\gamma_i LS) , \tag{6}$$

where $\phi(\gamma_i LS)$ is a configuration-state function with a specific coupling scheme and the c's are the configuration mixing coefficients. If in Eq. (6) only one dominant single configuration state function is considered, the MCHF calculations reduce to HF calculations. In the expansion of the total wave function ψ, singly and doubly excited configuration states are major contributions to the corre-

TABLE III. The expansion coefficients for the initial-state ^4D wave function in Kr^+.

Number	Coefficient	Configuration states
1	0.990 633 6	$4p^4(^3P)4d(^4D)$
2	0.025 266 1	$4p^3(^2P)4d(^3P)4f(^4D)$
3	−0.027 857 7	$4p^3(^2P)4d(^3D)4f(^4D)$
4	−0.018 518 9	$4p^3(^2D)4d(^3P)4f(^4D)$
5	0.051 031 4	$4p^3(^2D)4d(^3D)4f(^4D)$
6	0.023 724 4	$4p^3(^2D)4d(^3F)4f(^4D)$
7	0.028 353 2	$4p^3(^2D)4d(^3G)4f(^4D)$
8	−0.040 842 3	$4p^3(^4S)4d(^3D)4f(^4D)$
9	−0.012 808 6	$4p^3(^4S)4d(^5D)4f(^4D)$
10	0.010 079 8	$4p^3(2P)4d(^3P)5p(^4D)$
11	−0.016 952 7	$4p^3(^2P)4d(^3F)5p(^4D)$
12	0.007 604 8	$4p^3(^2D)4d(^3P)5p(^4D)$
13	−0.008 189 5	$4p^3(^2D)4d(^3D)5p(^4D)$
14	−0.015 392 4	$4p^3(^2D)4d(^3F)5p(^4D)$
15	−0.007 513 5	$4p^3(^4S)4d(^3D)5p(^4D)$
16	−0.006 043 4	$4p^3(^2P)4f(^3D)5d(^4D)$
17	−0.007 117 9	$4p^3(^2P)4f(^3F)5d(^4D)$
18	0.019 293 2	$4p^3(^2P)4f(^3G)5d(^4D)$
19	0.005 525 8	$4p^3(^2D)4f(^3F)5d(^4D)$
20	0.022 743 5	$4p^3(^2D)4f(^3G)5d(^4D)$
21	0.009 279 8	$4p^3(^4S)4f(^3F)5d(^4D)$
22	0.018 898 3	$4p^3(^4S)4f(^5F)5d(^4D)$
23	−0.013 936 3	$4p^2(^1S)4d^2(^3P)5d(^4D)$
24	−0.016 177 1	$4p^2(^1D)4d^2(^3P)5d(^4D)$
25	0.013 952 0	$4p^2(^1D)4d^2(^3F)5d(^4D)$
26	0.013 290 3	$4p^2(^1D)4d^2(^3P)5d(^4D)$
27	−0.026 608 1	$4p^2(^1D)4d^2(^3F)5d(^4D)$
28	−0.020 561 4	$4p^2(^3P)4d^2(^3F)5d(^4D)$
29	−0.023 835 1	$4p^3(^2P)5p(^3P)5d(^4D)$
30	0.027 722 5	$4p^3(^2D)5p(^3P)5d(^4D)$
31	−0.008 290 4	$4p^2(^1S)4d(^2D)4f^2(^4D)$
32	0.011 023 9	$4p^2(^1D)4d(^2D)4f^2(^4D)$
33	−0.009 019 1	$4p^2(^3P)4d(^4D)5s^2(^4D)$
34	0.012 236 0	$4p^2(^1D)4d(^2D)5p^2(^4D)$
35	0.014 634 6	$4p^2(^1D)4d(^2F)5p^2(^4D)$
36	0.018 309 8	$4p^2(^3P)4d(^4D)5p^2(^4D)$
37	−0.018 199 2	$4p^2(^3P)4d(^4D)5p^2(^4D)$
38	0.011 596 9	$4p^2(^1S)4d(^2D)5d^2(^4D)$
39	−0.015 585 3	$4p^2(^1D)4d(^2D)5d^2(^4D)$
40	−0.018 697 6	$4p^2(^1D)4d(^2F)5d^2(^4D)$
41	0.019 525 3	$4p^2(^1D)4d^3(^4P)(^4D)$
42	−0.055 432 8	$4p^2(^3P)4d^3(^2D)(^4D)$
43	−0.007 012 4	$4p^2(^3P)4d^3(^2P)(^4D)$

lation energy, as well as to the wave-function quality. Through the variations of MCHF orbitals, a basis for the presentation of the state of interest is obtained which is used to evaluate the atomic quantity. One could, in principle, use the same MCHF expansion to include relativistic effects through the Breit-Pauli calculations [37], but we do not investigate such relativistic effects in the present calculation of the SMS, since those contributions are smaller than the accuracy of the measurements.

We present the wave-function expansions of the lower $4p^4 4d\ ^4D$ and upper $4p^4 5p\ ^4P$ levels for the transition considered in Kr II. Separate MCHF calculations were performed for both of the final-term values ^4D and ^4P. For each term, couplings for the set of configurations $4p^4 4d$ and $4p^4 5p$ are generated with the specified final LS term. Because of the importance of these two configurations, they are referred to as the reference set. Additional configuration states included in the MCHF procedure are those that can be derived from the reference set through replacements of electrons to virtual orbits $4p$, $4d$, $5s$, $5p$, and $5d$. Such configuration states can potentially interact with one or more couplings derived from the above-mentioned reference set. All the orbitals, or so-called radial functions (including those from the core), were varied for both ^4D and ^4P states. The expansion coefficients for the initial ^4D wave functions are displayed in Table III. Because of the limitations on the MCHF code, we have used about 40 configurations in the expansion of the initial and final wave functions, which are shown in Tables III and IV. With these wave functions the matrix elements of the specific shift operator in Eq. (3) were separately calculated for the final and initial states. Then the results from the initial and final states were subtracted to determine the SMS for the transition

TABLE IV. The expansion coefficients for the final-state ^4P wave function in Kr^+.

Number	Coefficient	Configuration states
1	0.992 596 3	$4p^4(^3P)5p(^4P)$
2	0.032 117 0	$4p^3(^2D)5p(^3D)4f(^4P)$
3	0.037 714 2	$4p^3(^2D)5p(^3F)4f(^4P)$
4	−0.002 979 8	$4p^3(^2P)5p^2(^4P)$
5	0.025 646 0	$4p^3(^4S)5p^2(^4P)$
6	−0.017 211 8	$4p^3(^2P)4d(^3P)5s(^4P)$
7	0.029 880 7	$4p^3(^2D)4d(^3P)5s(^4P)$
8	0.009 272 2	$4p^3(^2P)4d(^3P)5d(^4P)$
9	−0.024 278 8	$4p^3(^2P)4d(^3D)5d(^4P)$
10	0.006 476 5	$4p^3(^2P)4d(^3F)5d(^4P)$
11	−0.017 683 6	$4p^3(^2D)4d(^3P)5d(^4P)$
12	0.017 703 9	$4p^3(^2D)4d(^3D)5d(^4P)$
13	0.005 895 1	$4p^3(^2D)4d(^3F)5d(^4P)$
14	−0.023 029 6	$4p^3(^4S)4d(^3D)5d(^4P)$
15	0.013 700 3	$4p^3(^2P)5s5d(^4P)$
16	−0.022 337 6	$4p^3(^2D)5s5d(^4P)$
17	0.010 881 8	$4p^3(^2P)4d^2(^4P)$
18	0.014 391 9	$4p^3(^2D)4d^2(^4P)$
19	0.022 263 0	$4p^3(^4S)4d^2(^4P)$
20	0.001 302 7	$4p^3(^2D)4d(^4P)$
21	−0.009 118 2	$4p^3(^2P)5d^2(^4P)$
22	−0.010 512 8	$4p^3(^2D)5d^2(^4P)$
23	−0.013 631 1	$4p^3(^4S)5d^2(^4P)$
24	−0.014 195 6	$4p^2(^1S)5p(^2P)4d5d(^4P)$
25	0.014 207 4	$4p^2(^1S)5p(^2P)4d5d(^4P)$
26	0.015 714 6	$4p^2(^1D)5p(^2P)4d5d(^4P)$
27	−0.015 577 0	$4p^2(^1D)5p(^2P)4d5d(^4P)$
28	−0.013 255 5	$4p^2(^1D)5p(^2D)4d5d(^4P)$
29	0.021 888 3	$4p^2(^1D)5p(^2D)4d5d(^4P)$
30	−0.029 717 2	$4p^2(^1D)5p(^2D)4d(^3F)5d(^4P)$
31	0.011 507 3	$4p^2(^3P)5p(^2S)4d(^3D)5d(^4P)$
32	−0.011 016 3	$4p^2(^3P)5p(^2D)4d(^3F)5d(^4P)$
33	0.020 495 5	$4p^2(^3P)5p(^4S)4d(^3D)5d(^4P)$
34	0.015 304 6	$4p^2(^3P)5p(^4S)4d(^5D)5d(^4P)$
35	−0.022 471 4	$4p^2(^3P)5p(^4P)4d(^3D)5d(^4P)$
36	0.027 640 6	$4p^2(^3P)5p(^4P)4d(^3F)5d(^4P)$
37	−0.014 377 6	$4p^2(^3P)5p(^4P)4d(^5P)5d(^4P)$
38	0.039 246 2	$4p^2(^3P)5p(^4P)4d(^5D)5d(^4P)$
39	0.014 402 9	$4p^2(^1D)5p(^2D)4f^2(^3P)(^4P)$
40	−0.006 762 3	$4p^2(^3P)5p(^4P)5s^2(^4P)$
41	−0.006 102 3	$4p^2(^3P)5p^3(^2D)(^4P)$

TABLE V. A comparison of the calculated and the experimentally observed SMS. (To obtain the SMS, the calculated NMS was subtracted from the observed total IS assuming that the FS is negligibly small.)

Isotope pairs	NMS (MHz)	SMS (HF) (MHz)	SMS (MCHF) (MHz)	SMS (Expt.) (MHz)
84-86	62.0	−485.7	−426.5	−418.2(8.0)
82-84	65.0	−509.4	−447.3	−438.6(5.0)
80-82	68.3	−534.8	−469.6	−463.7(10.0)
78-80	71.8	−562.3	−493.7	−489.5(10.0)

considered. All the correlations from the outer $4p$, $4d$, $4f$, $5s$, and $5d$ orbitals were taken into account. The reduced mass correction to the SMS was also included and yielded in the case of Kr^+ a Rydberg constant of 109 736.59 cm^{-1}.

The results of the HF and MCHF calculations for the SMS are compiled in Table V. It is clear from this table that the HF results, alone, are too large. However, they show that significant contributions come from the core momentum correlations of the electrons. When the correlations from the excitations of the outer electrons are added, the SMS results are somewhat reduced.

The final results of the MCHF calculations are also compared to the measured SMS values for the different isotope pairs in the last column of Table IV. The MCHF values are in good agreement with the experimental results. The MCHF results may improve further if correlations from the core electrons are included.

IV. CONCLUSIONS

Isotope shifts and hyperfine splittings were measured in the $4p^4 4d\ ^4D_{7/2} - 4p^4 5p\ ^4P^\circ_{5/2}$ transition for all the stable Kr isotopes between $A = 78$ and 86. The transition reveals a large isotope shift, which is mainly due to the specific-mass effect. HF and MCHF calculations for the specific-mass shift were carried out. The HF calculations show that important contributions to the SMS come from the core momentum correlations of the electrons. The MCHF calculations, which underline the importance of using accurate wave functions, are in excellent agreement with the experiment.

The large isotope shifts observed might also be useful for further improvement in the techniques devised for the sensitive detection of ^{81}Kr and ^{85}Kr. They could conceivably be exploited in improving the isotopic selectivity in some of these methods.

ACKNOWLEDGMENTS

This work was supported by DOE under Contract No. DE-AS05-80ER10578, the Teledyne Research Assistance Program, the Center for Energy and Mineral Resources at Texas A&M University, the Natural Science and Engineering Research Council of Canada (NSERC), and a NATO International Collaboration grant.

[1] B. D. Cannon and G. R. Janik, Phys. Rev. A **42**, 397 (1990) and references therein.

[2] T. J. Scholl, T. D. Gaily, R. A. Holt, and S. D. Rosner, Phys. Rev. A **33**, 2396 (1986).

[3] J. R. Brandenberger, Phys. Rev. A **39**, 64 (1989) and references therein.

[4] T. Trickl, M. J. J. Vrakking, E. Cromwell, Y. T. Lee, and A. H. Kung, Phys. Rev. A **39**, 2948 (1989) and references therein.

[5] N. Thonnard, R. D. Willis, M. C. Wright, W. A. Davis, and B. E. Lehmann, Nucl. Instrum. Methods Phys. Res. Sect. B **29**, 398 (1987).

[6] S. A. Aseyev, Y. A. Kudryavtsev, V. S. Letokhov, and V. V. Petrunin, J. Phys. B **24**, 2755 (1991).

[7] B. D. Cannon and T. J. Whitaker, Appl. Phys. B **38**, 57 (1985).

[8] G. R. Janik, B. D. Cannon, R. Ogorzalek-Loo, and B. A. Bushaw, J. Opt. Soc. Am. B **6**, 1617 (1989).

[9] G. R. Janik, B. A. Bushaw, and B. D. Cannon, Opt. Lett. **14**, 266 (1989).

[10] J. J. Snyder, T. B. Lucatorto, P. H. Debenham, and S. Geltman, J. Opt. Soc. Am. B **2**, 1497 (1985).

[11] J. J. Snyder, T. B. Lucatorto, P. H. Debenham, R. E. Bonanno, and C. W. Clark, in *Laser Spectroscopy VII,* Proceedings of the Seventh International Conference on Laser Spectroscopy, Hawaii, 1985, edited by T. W. Hänsch and Y. R. Shen (Springer-Verlag, Berlin, 1985), pp. 389–390.

[12] R. Davis, A. K. Mann, and L. Wolfenstein, Annu. Rev. Nucl. Part. Sci. **39**, 467 (1989).

[13] C. H. Chen, G. S. Hurst, and M. G. Payne, in *Progress in Atomic Spectroscopy,* edited by H. J. Beyer and H. Kleinpoppen (Plenum, New York, 1984), Part C, pp. 115–150.

[14] B. E. Lehmann, in *Analytical Laser Spectroscopy* (Ninth International School of Quantum Electronics), Vol. 119 of *NATO Advanced Study Institute, Series B: Physics,* edited by S. Martelluci and A. N. Chester (Plenum, New York, 1985), pp. 203–212.

[15] *Resonance Ionization Spectroscopy (RIS) 1990,* Proceedings of the Fifth International Symposium on Resonance Ionization Spectroscopy and its Applications, Varese, Italy, 1990, edited by J. E. Parks and N. Omenetto, IOP Conf. Proc. No. 114 (Institute of Physics, Bristol, England, 1991).

[16] *Resonance Ionization Spectroscopy (RIS) 1988,* Proceedings of the Fourth International Symposium on Resonance Ionization Spectroscopy and its Applications, Gaithersburg, US, 1988, edited by T. B. Lucatorto and J. E. Parks, IOP Conf. Proc. No. 94 (Institute of Physics, Bristol, England, 1989).

[17] *Resonance Ionization Spectroscopy (RIS) 1986,* Proceedings of the Third International Symposium on Resonance Ionization Spectroscopy and its Applications, Swansea, Wales, United Kingdom, 1986, edited by G. S. Hurst and C. Grey Morgan, IOP Conf. Proc. No. 84 (Institute of Physics, Bristol, England, 1987).

[18] *Resonance Ionization Spectroscopy (RIS) 1984,* Proceedings of the Second International Symposium on Resonance Ionization Spectroscopy and its Applications, Knoxville, Tennessee, 1984, edited by G. S. Hurst and M. G. Payne, IOP Conf. Proc. No. 71 (Institute of Physics, Bristol, England, 1984).

[19] H. A. Schuessler, R. M. Evans, Y. F. Li, S. D. Sledge, A. Alousi, and F. Buchinger, Third International Conference on Trends in Quantum Electronics, Bucharest, 1988, edited by A. M. Prokhorov and I. Ursu [SPIE Proc. **1033**, 488 (1989)].

[20] A. Eichhorn, M. Elbel, W. Kamke, R. Quad, and J. Bauche, Z. Phys. A **305**, 39 (1982).

[21] G. Borghs, P. De Bisschop, R. E. Silverans, M. Van Hove, and J. M. Van den Cruyce, Z. Phys. A **299**, 11 (1981).

[22] C. R. Bingham, M. L. Gaillard, D. J. Pegg, H. K. Carter, R. L. Mlekodaj, J. D. Cole, and P. M. Griffin, Nucl. Instrum. Methods **202**, 147 (1982).

[23] K. Heilig and A. Steudel, At. Data. Nucl. Data Tables **14**, 613 (1974).

[24] R. Neugart, in *Progress in Atomic Spectroscopy,* edited by H. J. Beyer and H. Kleinpoppen (Plenum, New York, 1987), Part D, pp. 75–127.

[25] H. A. Schuessler, A. Alousi, R. M. Evans, M. Brieger, F. Buchinger, and Y. F. Li, Phys. Rev. Lett. **65**, 1332 (1990).

[26] M. Menzinger and L. Wåhlin, Rev. Sci. Instrum. **40**, 102 (1969).

[27] W. Hofer, W. Vanek, P. Varga, and H. Winter, Rev. Sci. Instrum. **54**, 150 (1983).

[28] W. Schade, Z. W. Stryla, V. Helbig, and G. Langhans, Phys. Scr. **39**, 246 (1989).

[29] H. Kopfermann, *Nuclear Moments* (Academic, New York, 1958).

[30] A. Steudel, in *Hyperfine Interactions,* edited by A. J. Freeman and R. B. Frankel (Academic, New York, 1967), pp. 141–224.

[31] W. H. King, J. Opt. Soc. Am. **53**, 638 (1963).

[32] D. S. Hughes and C. Eckart, Phys. Rev. **36**, 694 (1930).

[33] J. P. Vinti, Phys. Rev. **56**, 1120 (1939); **58**, 882 (1940).

[34] C. Froese Fischer, Comput. Phys. Commun. **14**, 145 (1978).

[35] C. Froese Fischer, J. B. Lagowski, and S. H. Vosko, Phys. Rev. Lett. **59**, 2263 (1987).

[36] C. Froese Fischer and M. Idrees, Phys. Scr. **39**, 70 (1989).

[37] M. Idrees and C. Froese Fischer, Nucl. Instrum. Methods Phys. Res. B **42**, 552 (1989).

[38] C. Froese Fischer and L. Smentek-Mielczarek, J. Phys. B **16**, 3479 (1983).

[39] C. Froese Fischer, Phys. Rev. A **41**, 3481 (1990).

[40] E. Lindroth, A.-M. Mårtensson-Pendrill, and S. Salomonson, Phys. Rev. A **31**, 58 (1985).

[41] N. Vaeck, M. Godefroid, and C. Froese Fischer (unpublished).